

Intestinal CYP3A4 protects against lithocholic acid-induced hepatotoxicity in intestine-specific VDR-deficient mice^S

Jie Cheng,^{1,*†} Zhong-Ze Fang,^{1,*} Jung-Hwan Kim,^{*} Kristopher W. Krausz,^{*} Naoki Tanaka,^{*} John Y. L. Chiang,[†] and Frank J. Gonzalez^{2,**}

Laboratory of Metabolism,^{*} Center for Cancer Research, National Cancer Institute, National Institutes of Health, Bethesda, MD 20892; and Department of Integrative Medical Sciences,[†] Northeast Ohio Medical University, Rootstown, OH 44272

Abstract Vitamin D receptor (VDR) mediates vitamin D signaling involved in bone metabolism, cellular growth and differentiation, cardiovascular function, and bile acid regulation. Mice with an intestine-specific disruption of VDR (*Vdr*^{ΔIEpC}) have abnormal body size, colon structure, and imbalance of bile acid metabolism. Lithocholic acid (LCA), a secondary bile acid that activates VDR, is among the most toxic of the bile acids that when overaccumulated in the liver causes hepatotoxicity. Because cytochrome P450 3A4 (CYP3A4) is a target gene of VDR-involved bile acid metabolism, the role of CYP3A4 in VDR biology and bile acid metabolism was investigated. The *CYP3A4* gene was inserted into *Vdr*^{ΔIEpC} mice to produce the *Vdr*^{ΔIEpC}/*3A4* line. LCA was administered to control, transgenic-CYP3A4, *Vdr*^{ΔIEpC}, and *Vdr*^{ΔIEpC}/*3A4* mice, and hepatic toxicity and bile acid levels in the liver, intestine, bile, and urine were measured. VDR deficiency in the intestine of the *Vdr*^{ΔIEpC} mice exacerbates LCA-induced hepatotoxicity manifested by increased necrosis and inflammation, due in part to over-accumulation of hepatic bile acids including taurocholic acid and taurodeoxycholic acid. Intestinal expression of CYP3A4 in the *Vdr*^{ΔIEpC}/*3A4* mouse line reduces LCA-induced hepatotoxicity through elevation of LCA metabolism and detoxification, and suppression of bile acid transporter expression in the small intestine. **■** This study reveals that intestinal CYP3A4 protects against LCA hepatotoxicity.—Cheng, J., Z-Z. Fang, J-H. Kim, K. W. Krausz, N. Tanaka, J. Y. L. Chiang, and F. J. Gonzalez. **Intestinal CYP3A4 protects against lithocholic acid-induced hepatotoxicity in intestine-specific VDR-deficient mice.** *J. Lipid Res.* 2014. 55: 455–465.

Supplementary key words bile acids • vitamin D receptor • metabolomics

Vitamin D receptor (VDR) is activated by 1 α ,25-dihydroxy-vitamin D₃, an active form of vitamin D₃, and mediates

This work was funded by the National Cancer Institute Intramural Research Program, and by grants R37DK058379 and R01DK044442 to J.Y.L.C. from the National Institute of Diabetes and Digestive and Kidney Diseases, National Institutes of Health.

Manuscript received 23 September 2013 and in revised form 10 December 2013.

Published, JLR Papers in Press, December 16, 2013

DOI 10.1194/jlr.M044420

vitamin D signaling in numerous physiological and pharmacological processes (1). VDR is abundantly expressed in kidney, intestine, and bone, but is expressed at low levels in most other tissues (2). Deficiency of VDR leads to hypocalcemia, hyperparathyroidism, rickets, osteomalacia, alopecia, uterine hypoplasia, and growth retardation, which might result from repression of calcium absorption due to downregulation of duodenal epithelial calcium channels (3–7). Recently, an intestine-specific VDR knockout mouse model (*Vdr*^{ΔIEpC}) was generated that is deficient of VDR in the small intestine and colon. These mice have abnormal body size, colon structure, and feces bile acid composition, and are more susceptible to experimentally-induced inflammatory bowel disease than WT mice (8). Feces metabolomics revealed decreased concentrations of taurine, taurocholic acid, taurodeoxycholic acid (TDCA), and cholic acid in *Vdr*^{ΔIEpC} mice. In addition to the spontaneous accumulation of bile acids in VDR-deficient mice, it was reported that VDR ligands inhibit bile acid synthesis and transcription of the gene encoding cholesterol 7 α -hydroxylase (CYP7A1) (9, 10). In bile duct-ligated mice, 1 α ,25-dihydroxy-vitamin D₃ administration decreased liver bile acid content, increased the expression of bile acid transporters, and repressed pro-inflammatory cytokine

Abbreviations: ALP, alkaline phosphatase; ALT, alanine aminotransferase; *Asbt*, apical sodium-dependent bile acid transporter; *Bsep*, bile salt export pump; CYP3A4, cytochrome P450 3A4; CYP7A1, cholesterol 7 α -hydroxylase; *Fxr*, farnesoid X receptor; *Ibabp*, ileal bile acid-binding protein; LCA, lithocholic acid; *Mrp*, multidrug resistance-associated protein; *Ntcp*, Na⁺-taurocholate cotransporting polypeptide; *Oatp*, organic anion transporting polypeptide; *Ost*, organic solute transporter; PCA, principal components analysis; PXR, pregnane X receptor; TDCA, taurodeoxycholic acid; TCA, taurocholic acid; T- α -MCA, tauro- α -muricholic acid; T-CDCA, tauro-chenodeoxycholic acid; Tg-3A4, transgenic-CYP3A4; UPLC, ultra-performance liquid chromatography; VDR, vitamin D receptor; *Vdr*^{ΔIEpC}, intestine-specific vitamin D receptor knockout mouse.

¹J. Cheng and Z-Z. Fang contributed equally to this work.

²To whom correspondence should be addressed:

e-mail: gonzalezf@mail.nih.gov.

^SThe online version of this article (available at <http://www.jlr.org>) contains supplementary data in the form of six figures.

expression (11), which might be through regulation of sulfotransferase 2A1 to control bile acid-disrupted sterol homeostasis (12). Therefore, VDR might play a crucial role in regulation of bile acid metabolism (13).

Lithocholic acid (LCA), a monohydroxy secondary bile acid, is formed by bacterial 7-dehydroxylation of the primary bile acid, chenodeoxycholic acid, and of the secondary bile acid, ursodeoxycholic acid. The consensus emerged that the acute and chronic toxicity of LCA resulted from the administration of pharmacological loads of LCA (14). LCA also appears to induce its own detoxification in the liver. In addition, LCA is a potent activator of VDR (15). VDR controls transcription of the gene encoding sulfotransferase, an enzyme responsible for detoxification of LCA in humans. It was suggested that LCA enters the colonic enterocyte, activates VDR, and thereby induces its own detoxification (15). LCA was also shown to induce hepatic CYP3A4, a target gene regulated by VDR that is involved in bile acid metabolism, notably the oxidation of bile acids (16).

Due to the critical function of VDR in bile acid regulation and the unknown mechanism of bile acid accumulation in $Vdr^{\Delta Epc}$ mice, $Vdr^{\Delta Epc}$ mice and $Vdr^{\Delta Epc}$ mice expressing CYP3A4 were used to investigate the effect of VDR and CYP3A4 on LCA-induced hepatotoxicity and bile acid metabolism. The CYP3A4 transgene was inserted into $Vdr^{\Delta Epc}$ mice through crossing transgenic-CYP3A4 (Tg-3A4) mice to $Vdr^{\Delta Epc}$ mice to establish a new line designated $Vdr^{\Delta Epc}/3A4$. LCA was administered to these mice and hepatotoxicity and bile acid metabolism and transport evaluated; while metabolomics, a high-throughput technology platform to measure metabolic fluctuations in exogenous and endogenous compounds (17), was employed to investigate bile flux changes in the gastrointestinal system. The results revealed that VDR deficiency in the intestine increases LCA-induced liver necrosis due to over-accumulation of hepatic bile acids. CYP3A4 alleviates LCA-induced hepatotoxicity through the suppression of bile acid transporters and escalation of LCA detoxification.

METHODS

Generation of $Vdr^{\Delta Epc}/3A4$ mice

$Vdr^{\Delta Epc}$ and Tg-3A4 mice were housed in temperature- and light-controlled rooms and were given water and pelleted chow ad libitum. $Vdr^{\Delta Epc}$ founders were mated to Tg-3A4 mice and the litters were genotyped and divided into four groups: WT ($Vdr^{fl/fl, cre^-}/3A4^-$), Tg-3A4 ($Vdr^{fl/fl, cre^-}/3A4^+$), $Vdr^{\Delta Epc}$ ($Vdr^{fl/fl, cre^+}/3A4^-$), and $Vdr^{\Delta Epc}/3A4$ ($Vdr^{fl/fl, cre^+}/3A4^+$). All groups of mice used in this study were obtained from these same littermates. All animal experiments were carried out in accordance with the Institute of Laboratory Animal Resources guidelines and approved by the National Cancer Institute Animal Care and Use Committee.

Experimental design

Two- to three-month-old WT, Tg-3A4, $Vdr^{\Delta Epc}$, and $Vdr^{\Delta Epc}/3A4$ male mice were fed AIN-93G purified diets for 3 days, followed by LCA (0.6% w/w) mixed in the AIN-93G purified diet for 4 days.

Serum samples were collected and mice were euthanized by CO₂ asphyxiation. Urine, liver, duodenum, jejunum, ileum, colon, and other tissue samples were harvested and stored at -80°C for analysis.

Assessment of liver injury

For assessment of macroscopic liver damage, liver tissue was flushed with PBS and fixed in 10% buffered formalin. Liver injury was scored by double-blinded analysis on a routine hematoxylin and eosin-stained section according to the morphological criteria previously described (18). Drug-induced liver injury was further evaluated by measuring alanine aminotransferase (ALT) and alkaline phosphatase (ALP) in serum. Briefly, 2 μ l of serum was mixed with 200 μ l of ALT or ALP assay buffer (Catachem, Bridgeport, CT) in a 96-well microplate, and the oxidation of NADH to NAD⁺ was monitored at 340 nm for 5 min.

Cholesterol and bile acid uptake measurements

Plasma levels of total cholesterol in serum and liver homogenate were measured in overnight-fasted mice using assay kits from Wako Diagnostics (Richmond, VA). Liver homogenate was extracted as follows: 20 mg liver was homogenized with 200 μ l extraction buffer [50 mM Tris/HCL, 1% Triton X-100 (v/v)]. One microliter of supernatant was used for the measurements as described for serum analysis according to the manufacturer's protocol (Wako USA, Richmond, VA). To measure the hepatic and enteric bile acid levels, 20 mg of frozen liver or mucosa cells scraped from the entire intestine were homogenized in 400 μ l of 75% ethanol, incubated at 50°C for 2 h, and then centrifuged. The supernatant (aqueous fraction) was retained, evaporated, and resuspended in 200 μ l of 0.9% saline. Twenty microliters were used for bile acid quantification using the VetSpec bile acids kit (Catachem, Oxford, CT).

RNA analysis

Hepatic and intestinal RNA was extracted using TRIzol reagent (Invitrogen, Carlsbad, CA) and quantitative (q)PCR performed using cDNA generated from 1 μ g of total RNA with SuperScript II reverse transcriptase (Invitrogen). Primers for qPCR were designed using the Primer Express software (Applied Biosystems, Foster City, CA) and sequences are available upon request. qPCR reactions were carried out using SYBR Green PCR master mix (SuperArray, Frederick, MD) by using an ABI Prism 7900HT sequence detection system (Applied Biosystems). Values were quantitated using the comparative cycle threshold method, and results were normalized to mouse β -actin.

Metabolomics analysis of urine, bile, and tissue homogenates

Urine samples were processed by mixing 40 μ l of urine with 160 μ l of 50% aqueous acetonitrile and centrifuging at 18,000 g for 10 min to remove protein and particulates. Liver tissues (100 mg) were homogenized on the ice, and 1 ml acetonitrile:water (50% v:v) was added for denaturation of protein. After multiple centrifugations, supernatants were collected. Bile samples were denatured by a 100-fold dilution with acetonitrile:water (66% v:v) and supernatants processed for liquid chromatography analysis. The homogenates of small intestine tissues (duodenum, jejunum, and ileum) were prepared and diluted with 1:20 acetonitrile:water (50% v:v). Supernatants were injected into an ultra-performance liquid chromatography (UPLC) system (Waters Corporation, Milford, MA) and metabolites separated by a gradient ranging from water to 95% aqueous acetonitrile containing 0.1% formic acid over a 10 min run. An Acquity UPLCTM BEH C18 column (Waters Corporation) was used to separate chemical components at 35°C.

The mobile phase flow rate was 0.5 ml/min with an aqueous acetonitrile gradient containing 0.1% formic acid over a 10 min run (0% acetonitrile for 0.5 min to 20% acetonitrile by 5 min to 95% acetonitrile by 9 min, then equilibration at 100% water for 1 min before the next injection). The QTOF Premier™ mass spectrometer was operated in the positive electrospray ionization mode. Capillary voltage and cone voltage were maintained at 3 kV and 20 V, respectively. Source temperature and desolvation temperature were set at 120°C and 350°C, respectively. Nitrogen was used as both cone gas (50 l/h) and desolvation gas (600 l/h), and argon was used as collision gas. For accurate mass measurements, the TOFMS was calibrated with sodium formate solution (range m/z 100–1,000) and monitored by the intermittent injection of the lock mass sulfadimethoxine ($[M+H]^+ = m/z$ 311.0814) in real-time. Mass chromatograms and mass spectral data were acquired and processed by MassLynx software (Waters Corporation) in centroid format.

Quantitation of metabolites

LCA, LCA metabolites, and bile acid standards were purchased from Sigma-Aldrich. Quantitation of bile acid metabolites was performed using an ACQUITY UPLC system coupled with a XEVO triple-quadrupole tandem mass spectrometer (Waters Corporation). The detection and quantitation of biomarkers were accomplished by multiple reaction monitoring mass spectrometry.

Metabolomic data analysis

Chromatographic and spectral data were deconvoluted by MarkerLynx software (Waters Corporation). A multivariate data matrix containing information on sample identity, ion identity (retention time and m/z), and ion abundance was generated through centroiding, deisotoping, filtering, peak recognition, and integration. The intensity of each ion was calculated by normalizing the single ion counts versus the total ion counts in the whole chromatogram. The data matrix was further exported into SIMCA-P™ software (Umetrics, Kinnelon, NJ) and transformed by mean-centering and Pareto scaling, a technique that increases the importance of low abundance ions without significant amplification of noise. Principal components of serum were generated by principal components analysis (PCA) to represent the major latent variables in the data matrix and were described in a scores scatter plot.

In vitro incubation system for investigation of intestinal LCA phase I metabolism

Mouse intestinal microsomes obtained from WT and Tg-3A4 mice were prepared. The phase I incubation system (200 μ l) contained 50 mM Tris-HCl buffer solution (pH 7.4), 0.5 mg/ml mouse intestinal microsomes, 5 mM MgCl₂, 100 μ M LCA, and 1 mM freshly prepared NADPH. After 0.5 h incubation at 37°C, the reaction was stopped using 200 μ l cold 50% aqueous methanol containing 5 μ M chlorpropamide. After centrifuging at 14,000 g for 20 min, a 5 μ l aliquot of the supernatant was injected into a UPLC-ESI-QTOFMS. An Acquity C18 BEH UPLC column (Waters Corporation) was employed to separate components in serum, urine, feces, and microsomal incubation samples. The mobile phase consisted of water containing 0.1% formic acid (A) and acetonitrile containing 0.1% formic acid (B). The following gradient condition was used: 100% A for 0.5 min, increased to 100% B over the next 7.5 min, and returned to 100% A in the last 2 min. The flow rate of the mobile phase was set at 0.5 ml/min. Data were collected in negative ion mode on a Waters QTOF Premier mass spectrometer, which was operated in full-scan mode at m/z 50–850. Nitrogen was used as both cone gas (50 l/h) and desolvation gas (600 l/h). Source desolvation temperatures

were set at 120°C and 350°C, respectively. The capillary voltage and cone voltage were 3,000 and 20 V, respectively.

Western blotting

Mouse ileums were lysed with RIPA lysis buffer [150 mM NaCl, 0.5% Triton X-100, 50 mM Tris-HCl (pH 7.4), 25 mM NaF, 20 mM EGTA, 1 mM DTT, 1 mM Na₃VO₄, and protease inhibitor cocktail] for 30 min on ice, followed by centrifugation at 14,800 g for 15 min. Protein concentrations were measured with bicinchoninic acid (BCA) reagent. Protein (30–60 μ g) was electrophoresed on a 4–15% gradient Tris-HCl gel (Bio-Rad, Hercules, CA) and transferred onto a polyvinylidene difluoride membrane in Tris-glycine buffer (pH 8.4) containing 20% methanol. The membrane was blocked with 5% fat-free dry milk in phosphate-buffered saline containing 0.1% Tween-20 (PBST) for 1 h. The membranes were probed with primary antibodies and horseradish peroxidase-conjugated secondary antibodies using standard Western blotting procedures. Proteins were visualized using the Femto signal chemiluminescent substrate (Pierce) under the image analyzer (Alpha Innotech Corp., San Leandro, CA). The antibody to mouse apical sodium-dependent bile acid transporter (ASBT) was generously supplied by Paul A. Dawson, Wake Forest University School of Medicine.

Statistics

Experimental values are expressed as mean \pm SD. Statistical analysis was performed with two-tailed Student's t -tests with $P < 0.05$ considered statistically significant.

RESULTS

LCA-induced hepatotoxicity is alleviated in *Vdr*^{ΔIEpC} mice with CYP3A4 insertion

While the body weights of the *Vdr*^{ΔIEpC} mice are low, the body weights of the *Vdr*^{ΔIEpC}/3A4 mice are similar to the WT controls. The body weights of *Vdr*^{ΔIEpC} mice ranged from 16 to 20 g at 8 weeks of age, while the body weights of *Vdr*^{ΔIEpC}/3A4 mice ranged from 22 to 29 g, which is similar to the WT C57BL/6 mice on the same genetic background, thus suggesting that CYP3A4 rescues some of the abnormal phenotype of the *Vdr*^{ΔIEpC} mice (8). To investigate bile acid metabolism in *Vdr*^{ΔIEpC}/3A4 mice, LCA was administered for 4 days. LCA causes intrahepatic cholestasis and damage to the bile canaliculi in rodents (19). Histological results revealed that LCA caused severe hepatotoxicity with areas of necrosis of irregular distribution with some dilatation of centrolobular venules with inflammatory and neutrophil infiltration in WT, Tg-3A4, *Vdr*^{ΔIEpC}, and *Vdr*^{ΔIEpC}/3A4 mice (Fig. 1A). Liver injury was lower in Tg-3A4 mice compared with WT mice, and markedly reduced in *Vdr*^{ΔIEpC}/3A4 mice compared with *Vdr*^{ΔIEpC} mice as demonstrated by the reduced severity of lesion score ($P < 0.05$), coagulation necrosis ($P < 0.05$), biliary proliferation, inflammation cell infiltration, and portal inflammation (supplementary Fig. 1). Hepatotoxicity was most severe in *Vdr*^{ΔIEpC} mice compared with WT mice, and *Vdr*^{ΔIEpC}/3A4 mice compared with Tg-3A4 mice. Liver and kidney weights relative to body weights were high in *Vdr*^{ΔIEpC} mice, and these levels were lower in the *Vdr*^{ΔIEpC}/3A4 mice. Tg-3A4 mice alone showed a slight but significant decrease in liver

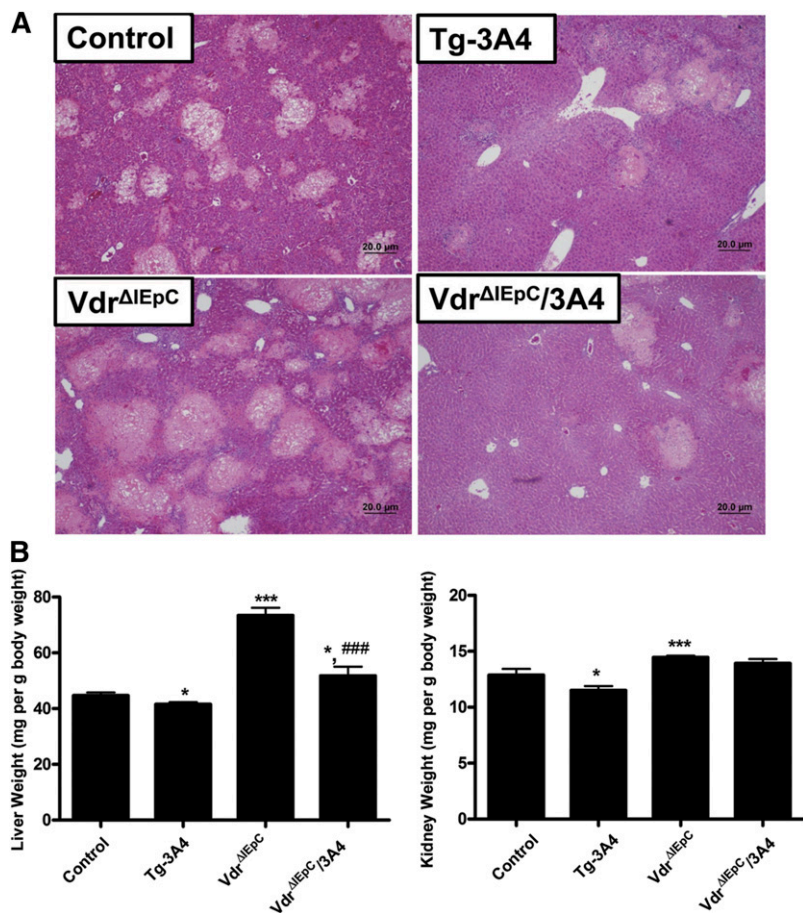


Fig. 1. Histological analysis of liver toxicity. A: Microscopic observation revealed that LCA administration caused severe hepatotoxicity with areas of necrosis of irregular distribution with some dilatation of centrilobular venules with inflammatory and neutrophil infiltration in WT, Tg-3A4, *Vdr*^{ΔIEpC}, and *Vdr*^{ΔIEpC}/3A4 mice. Liver injury is alleviated in Tg-3A4 compared with WT mice, as well as reduced in *Vdr*^{ΔIEpC}/3A4 mice compared with *Vdr*^{ΔIEpC} mice. B: Liver weight versus body weight and kidney weight versus body weight in *Vdr*^{ΔIEpC} and *Vdr*^{ΔIEpC}/3A4 mice. **P* < 0.05 compared with control in same group; ****P* < 0.001 compared with control in same group; ###*P* < 0.001 compared with *Vdr*^{ΔIEpC} in same group.

weight versus body weight and kidney weight versus body weight compared with controls (Fig. 1B).

Upon treatment with LCA, *Vdr*^{ΔIEpC} mice with or without the CYP3A4 gene had increased ALT and ALP values compared with WT and Tg-3A4 mice. The *Vdr*^{ΔIEpC}/3A4 mice had decreased ALT and ALP compared with *Vdr*^{ΔIEpC} mice, although there was a tendency toward lower without significant differences of ALT and ALP between control and Tg-3A4 mice (Fig. 2). These data suggested that intestinal VDR deficiency results in greater LCA hepatotoxicity and that CYP3A4 alleviates the hepatotoxicity induced by LCA in the intestinal *Vdr*-null background. Due to the potential effect of LCA hepatic metabolism, cholesterol and bile acid levels in liver and serum were measured. There were no significant differences in serum cholesterol levels between the four groups. In contrast, hepatic cholesterol was significantly increased in *Vdr*^{ΔIEpC} mice, and decreased in *Vdr*^{ΔIEpC}/3A4 mice (Fig. 2). Similarly, hepatic bile acids were increased in *Vdr*^{ΔIEpC} mice and decreased in *Vdr*^{ΔIEpC}/3A4 mice. However, enteric bile acids extracted from epithelial cells scraped from the entire intestine showed no significant difference between these mice, despite the slight increase of bile acids in *Vdr*^{ΔIEpC} mice compared with the other groups (Fig. 2). Moreover, the bile acid pool size was higher in *Vdr*^{ΔIEpC} mice compared with *Vdr*^{ΔIEpC}/3A4 mice, and the bile acid pool size in both groups of mice was higher than control and Tg-3A4 mice, while there was no significant difference between control and Tg-3A4 mice (Fig. 2). The mechanism for the lower

bile acid pool in the *Vdr*^{ΔIEpC}/3A4 mice is not known; it may be due to increased metabolism of bile acid intermediates by CYP3A4. Thus, LCA-induced hepatotoxicity might be aggravated in *Vdr*^{ΔIEpC} mice through induction of hepatic cholesterol and bile acid synthesis, and this is alleviated by intestinal detoxification by CYP3A4.

Gene and urinary metabolomic profiles reveal activation of CYP3A by LCA administration

Real-time qPCR analysis of LCA-treated mice showed that *CYP3A4* mRNA is highly expressed in the small intestine but not in the liver of Tg-3A4 and *Vdr*^{ΔIEpC}/3A4 mice (Fig. 3). VDR and pregnane X receptor (PXR), known inducers of *CYP3A4* (20), were also examined. While *CYP3A4* was expressed at lower levels in the duodenum of *Vdr*^{ΔIEpC}/3A4 mice as compared with Tg-3A4 mice, there was not much difference in the expression in other regions of the intestine. *Vdr* mRNA was similarly expressed at slightly higher levels in Tg-3A4 mice compared with *Vdr*^{ΔIEpC}/3A4 mice only in the duodenum; there were no significant differences in *Pxr* and farnesoid X receptor (*Fxr*) mRNA expression between the four treated groups, although they had higher levels in the liver compared with the intestine (Fig. 3). The role of CYP3A4 in LCA metabolism was then investigated with microsomes prepared from the intestine. The molecular ions $[M-H]^- = 375.29$ and $[M-H]^- = 391.28$ were used to extract the peak of LCA and its hydroxylated products produced in intestinal microsomes in vitro (supplementary Fig. IIA). Two hydroxylated products (M-1 and

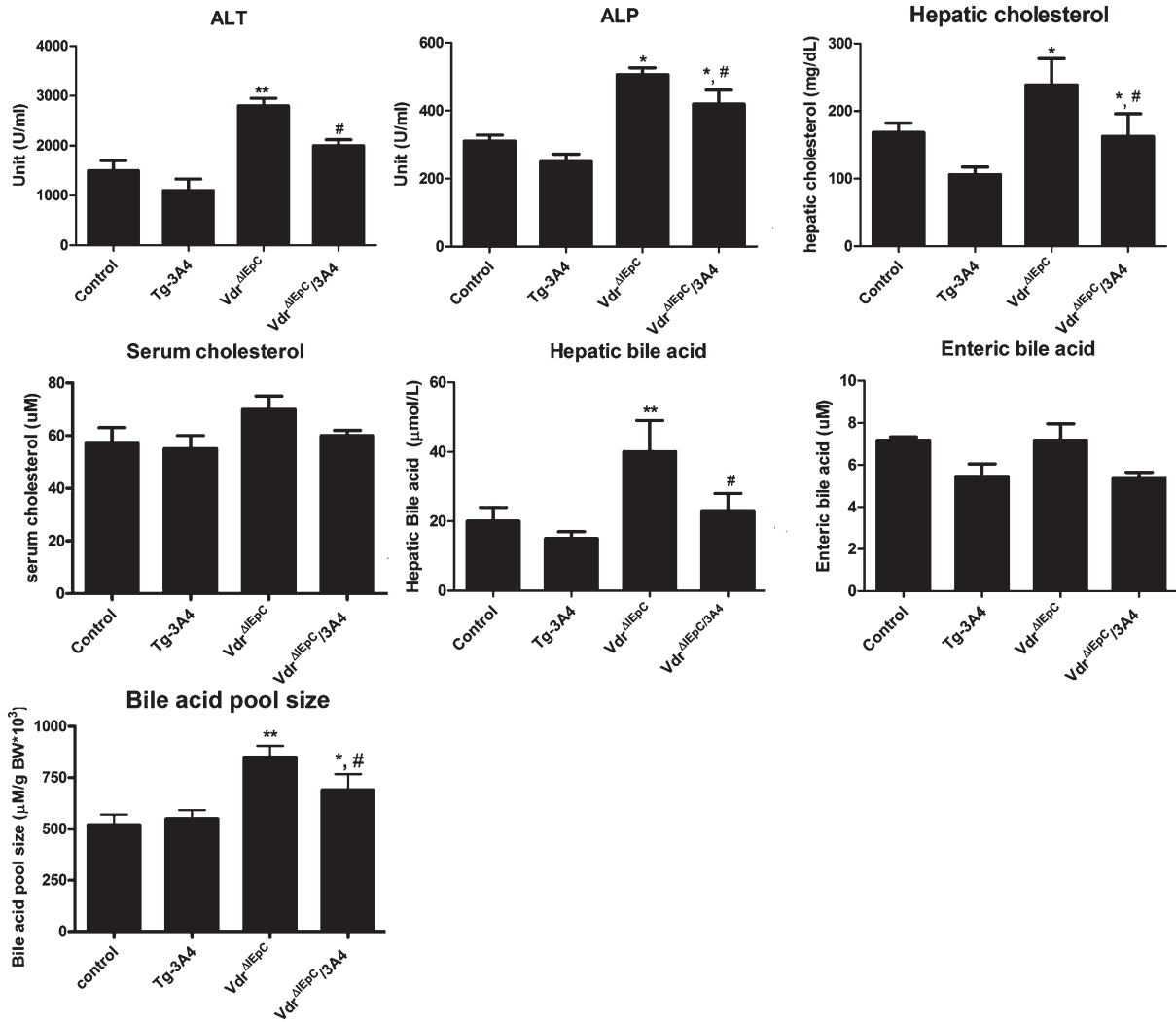


Fig. 2. Serum biochemistry of WT, Tg-3A4, *Vdr*^{ΔIEpC}, and *Vdr*^{ΔIEpC}/3A4 mice treated with LCA. ALP, ALT, serum cholesterol, hepatic cholesterol, hepatic bile acids, and enteric bile acids from mucosa cells scraped from the entire intestine in WT, Tg-3A4, *Vdr*^{ΔIEpC}, and *Vdr*^{ΔIEpC}/3A4 mice, as well as bile acid pool size in these four treated mice. * $P < 0.05$ compared with control in same group; ** $P < 0.01$ compared with control in same group; # $P < 0.05$ compared with *Vdr*^{ΔIEpC} in same group.

M-2) were identified, and a significant increase ($P < 0.001$) was detected for the formation M-1 in Tg-3A4 mice as compared to WT mice. An elevation trend was also observed for M-2 in Tg-3A4 mice (supplementary Fig. IIB). These data indicate that increased expression of CYP3A4 in Tg-3A4 stimulated metabolism of LCA in the intestine.

Metabolomic analysis of liver homogenate, small intestine homogenate, gallbladder, and urine

It was reported that increased LCA and LCA metabolites are correlated with elevated levels of bile acids (20–22). To investigate bile acid constituents, metabolomics was carried out on the four mouse groups treated with LCA. PCA revealed clear separation between urine metabolites in the control and treated group in positive or negative ionization modes in *Vdr*^{ΔIEpC} and *Vdr*^{ΔIEpC}/3A4 mice (supplementary Fig. IIIA). The model fit (R^2 value) and prediction powers (Q^2 value) of the PCA model indicated good separation of the PCA model. The loading plot

showed contribution ions I, II, III, and IV in positive mode were determined to be LCA, lithocholate-O-glucuronide, LCA glycine conjugate, and hydroxylated LCA, respectively, and ions V and VI in negative mode (supplementary Fig. IIIB) were lithocholytaurine and taurine, respectively, as revealed through MS/MS fragmentation and structure identification. These data indicate that the production of LCA metabolites through oxidation and conjugation is increased in *Vdr*^{ΔIEpC}/3A4 mice compared with *Vdr*^{ΔIEpC} mice, likely due to the involvement of CYP3A4.

It was reported that increased LCA and LCA metabolites are correlated with elevated levels of bile acids (20–22). To investigate the bile acid constituents, metabolomic analysis of liver and gallbladder bile was carried out. PCA of the hepatic metabolomes revealed a clear separation between control and Tg-3A4 mice, and *Vdr*^{ΔIEpC} and *Vdr*^{ΔIEpC}/3A4 mice (Fig. 4A). Moreover, loading plots from the PCA revealed that TDCA, taurocholic acid (TCA), tauro- α -muricholic acid (T- α -MCA), and tauro-chenodeoxycholic

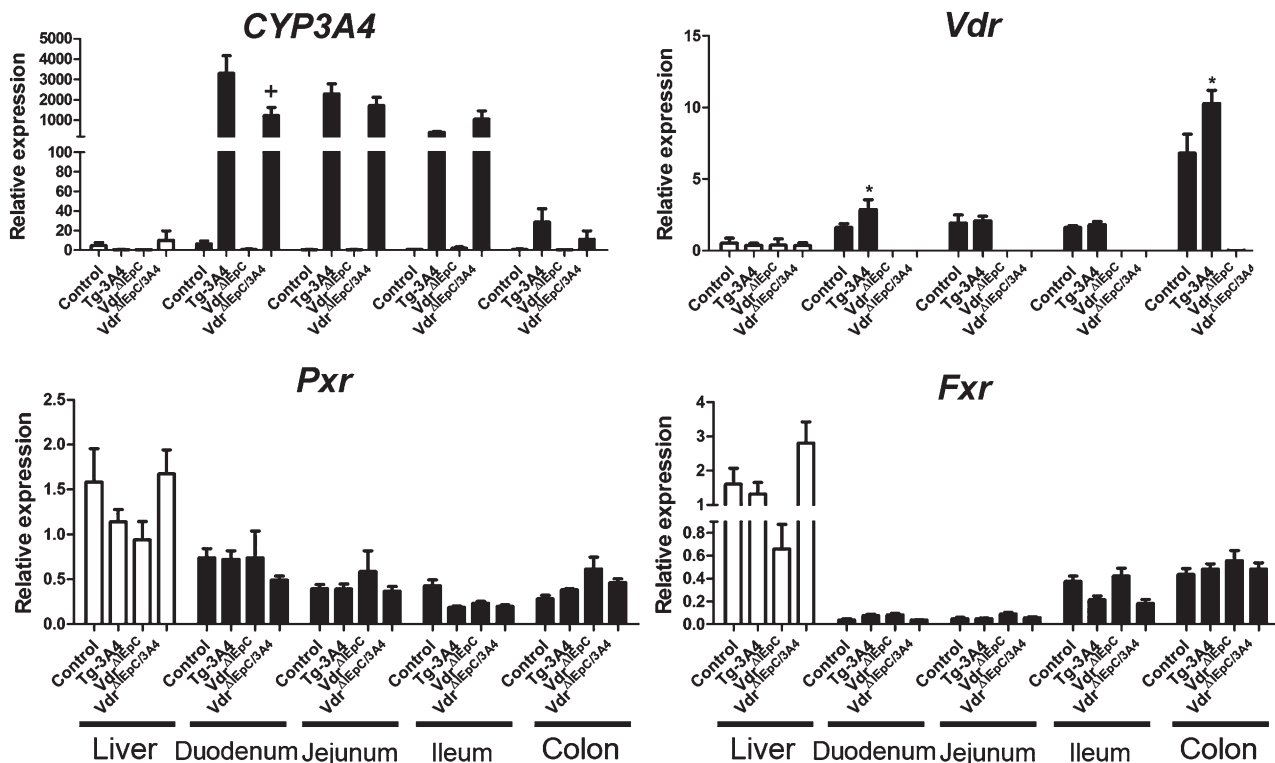


Fig. 3. Expression of mRNAs encoding enzymes responsible for LCA metabolism. *CYP3A4*, *Pxr*, *Fxr*, and *Vdr* mRNAs were measured by qPCR in WT, Tg-3A4, *Vdr*^{ΔIEpC}, and *Vdr*^{ΔIEpC}/3A4 mice. **P* < 0.05 compared with control mice in the same group; +*P* < 0.05 compared with control in Tg-3A4 group.

acid (T-CDCA) were the four major ions contributing to the distinctive clustering of *Vdr*^{ΔIEpC} from *Vdr*^{ΔIEpC}/3A4 mice in the negative mode. Quantitation of these four bile acids using specific ion monitoring and purified standards, revealed that TCA and TDCA are significantly higher in *Vdr*^{ΔIEpC} mice compared with the other three mouse lines, while TCA and TDCA are significantly decreased in *Vdr*^{ΔIEpC}/3A4 mice compared with *Vdr*^{ΔIEpC} mice (Fig. 4C). Tissue metabolomic analysis was carried out on intestine homogenates from WT and Tg-3A4 mice, and a similar trend, as noted with liver homogenates, was found in intestine homogenates, including a PCA separation trend between the two mouse lines (supplementary Fig. IV) and increased TCA levels in the duodenum and jejunum with a trend toward increase in the ileum (supplementary Fig. V). These results indicate that the high abundance of TCA and TDCA might be correlated with increased bile acid synthesis and metabolism and resulted in accumulation in *Vdr*^{ΔIEpC} mice and increased LCA-induced hepatotoxicity. Detoxification of LCA in *Vdr*^{ΔIEpC}/3A4 mice might be through LCA metabolism, and thus decreased the effect of LCA on specific bile acid accumulation in the liver and the circulation. Furthermore, PCA of the gallbladder bile revealed a clear separation between control and Tg-3A4 mice and *Vdr*^{ΔIEpC} and *Vdr*^{ΔIEpC}/3A4 mice (Fig. 4B). Moreover, loading plots from PCA revealed that TDCA, TCA, T-α-MCA, and T-CDCA are the four major ions contributing to the distinctive clustering of *Vdr*^{ΔIEpC} from *Vdr*^{ΔIEpC}/3A4 mice in negative mode, and the results were correlated with liver metabolomic analysis.

Expression of genes responsible for bile acid synthesis and transport

Although intestinal CYP3A4 detoxified LCA and reduced bile acid over-accumulation, bile acid accumulation might also influence bile acid synthesis and transport. Thus, expression from multiple transport genes, including *Asbt*, organic solute transporters α and β (*Osta* and *Ostβ*), multidrug resistance-associated proteins (*Mrp1*, *Mrp2*, and *Mrp3*), and organic anion transporting polypeptides (*Oatp1*, *Oatp2*, and *Oatp4*), in three regions of the intestine were evaluated by qPCR measurement of mRNAs (Fig. 5). Intestinal *Oatp1* and *Oatp4* mRNAs were decreased in *Vdr*^{ΔIEpC}/3A4 mice compared with *Vdr*^{ΔIEpC} mice, while there were no significant differences in *Mrp1*, *Mrp2*, and *Mrp3* mRNAs in the intestine. *Asbt* and *Osta* mRNAs were reduced in the intestine of *Vdr*^{ΔIEpC}/3A4 mice compared with *Vdr*^{ΔIEpC} mice (Fig. 5). Western blotting results further demonstrated that ASBT protein was more strikingly reduced than its mRNA by expression of CYP3A4 in the intestinal *Vdr*-null background (supplementary Fig. VI). Moreover, ileal bile acid-binding protein (*Ibabbp*) mRNA was increased in *Vdr*^{ΔIEpC}/3A4 mice compared with *Vdr*^{ΔIEpC} mice. Increasing IBABP may facilitate transport of bile acids to OSTs for efflux. Decreasing OSTs may reduce bile acid efflux, while increasing IBABP may compensate by more efficiently delivering bile acids to OSTs for efflux. In addition, bile acids are not absorbed into enterocytes and do not circulate back to the liver, so induction of IBABP favors reduction of intracellular bile acids as protection against LCA toxicity. Genes related to bile acid synthesis in

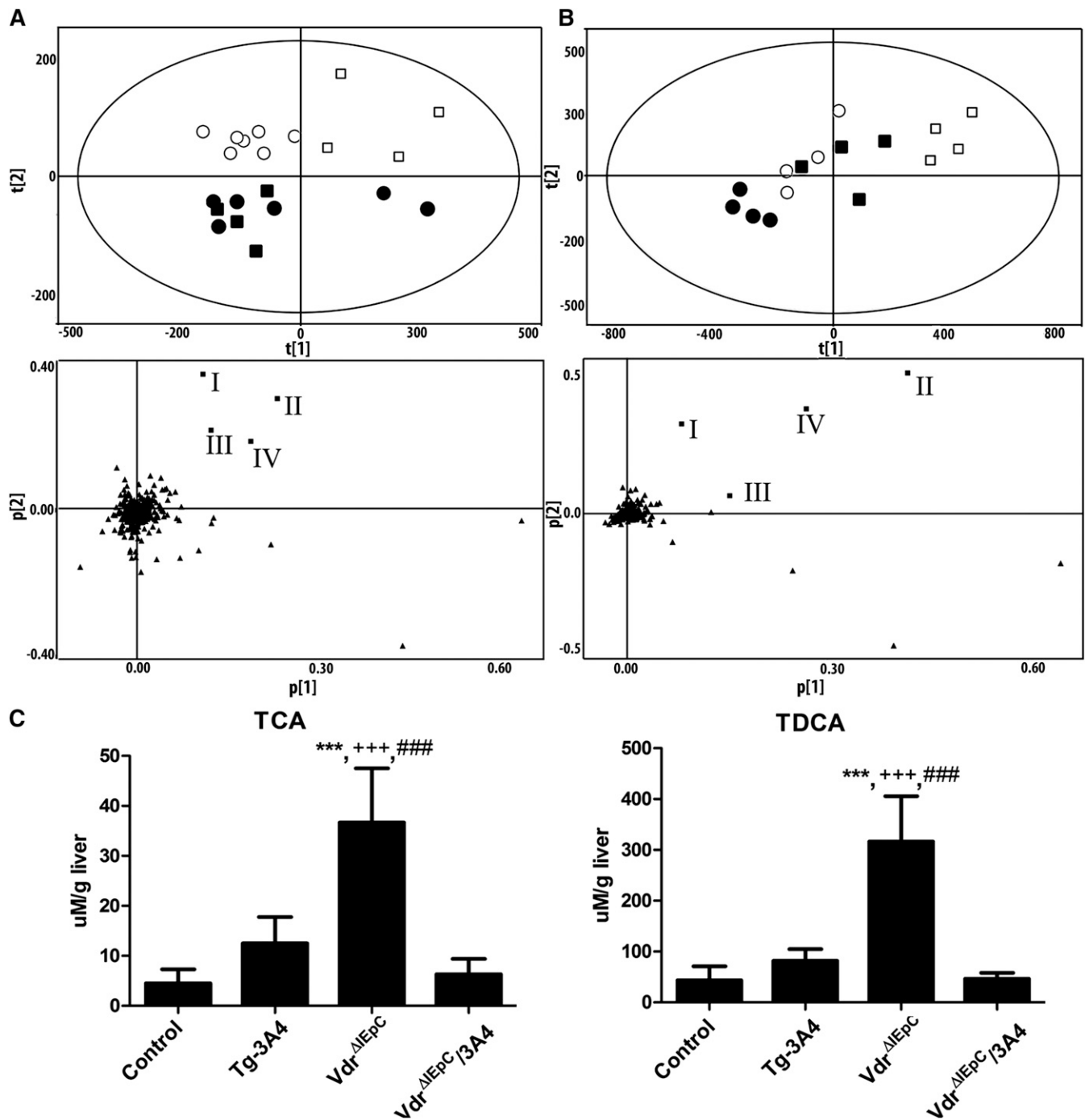


Fig. 4. Metabolomic analysis of liver homogenate and bile in negative mode from $Vdr^{\Delta EPC}$ and $Vdr^{\Delta EPC}/3A4$ mice. A: PCA (upper panel A) of the negative mode of liver homogenate metabolome revealed a clear separation of control (■), Tg-3A4 (●), $Vdr^{\Delta EPC}$ (□), and $Vdr^{\Delta EPC}/3A4$ (○). Loading plots (lower panel A) from the PCA showing four bile acid metabolites labeled with boxes: I, TDCA; II, taurocholic acid (TCA); III, T- α -MCA; and IV, T-CDCA contributing to the distinctive clustering of $Vdr^{\Delta EPC}$ from the other groups. B: PCA (upper panel B) of the negative bile metabolome revealed a clear separation of control (■), Tg-3A4 (●), $Vdr^{\Delta EPC}$ (□), and $Vdr^{\Delta EPC}/3A4$ (○). Loading plots (lower panel of B) from the PCA show the same four bile acid metabolites which are TCA, T-CDCA, TDCA and T- α -MCA, respectively. C: Quantitation of TCA and TDCA in liver homogenate from control, Tg-3A4, $Vdr^{\Delta EPC}$, and $Vdr^{\Delta EPC}/3A4$ mice. *** $P < 0.001$ compared with control in same group; +++ $P < 0.001$ compared with Tg-3A4 in same group; ### $P < 0.001$ compared with $Vdr^{\Delta EPC}/3A4$ in same group.

liver, including hepatic *Cyp8b1* and *Cyp7a1*, bile salt export pump (*Bsep*), and Na^+ -taurocholate cotransporting polypeptide (*Ntcp*), were also examined. The results demonstrated higher expression of *Bsep* and *Ntcp* mRNAs in $Vdr^{\Delta EPC}/3A4$ mice and a low expression level of *Cyp7a1* in $Vdr^{\Delta EPC}/3A4$ mice compared with $Vdr^{\Delta EPC}$ mice. Hepatic

Oatp2 demonstrated higher expression in $Vdr^{\Delta EPC}/3A4$ mice compared with $Vdr^{\Delta EPC}$ mice. Because *Bsep* is responsible for bile acid efflux from the liver to the gallbladder, *Ntcp* and *Oatp2* are involved in bile acid influx from the circulation to the liver; these data suggest that the decreased synthesis of bile acids by CYP7A1 in $Vdr^{\Delta EPC}/3A4$

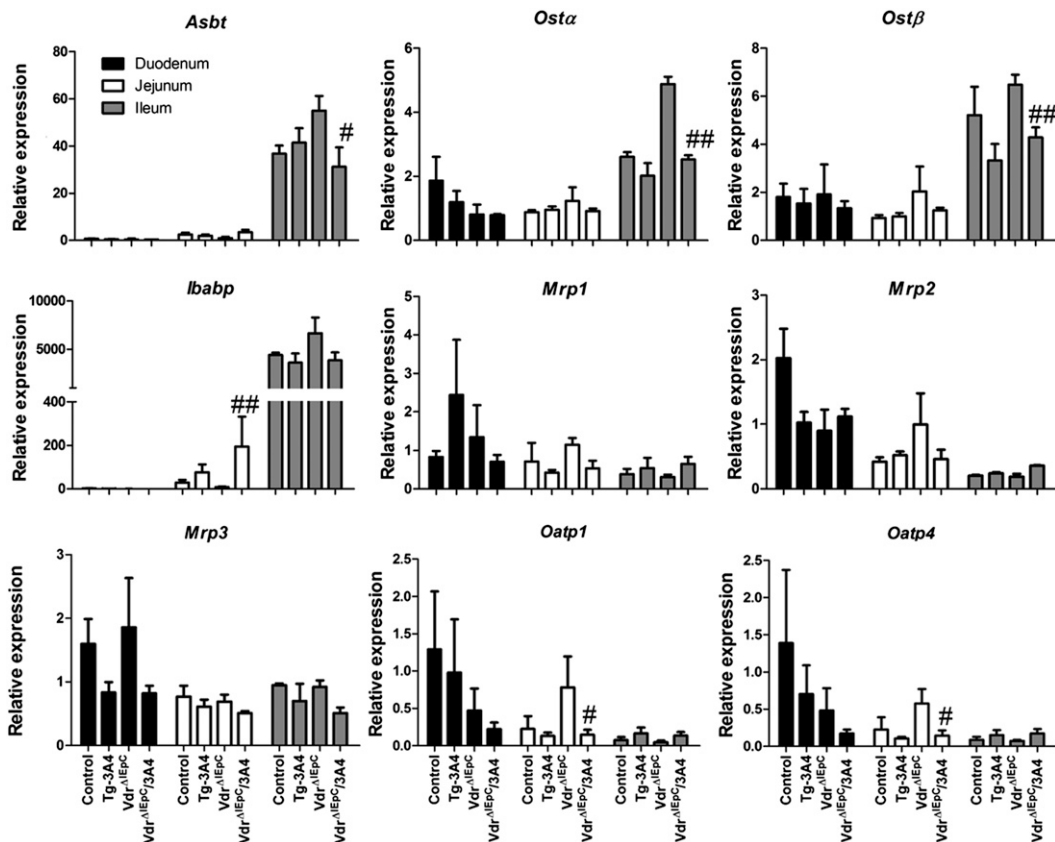


Fig. 5. Expression of mRNAs encoding enzymes responsible for bile acid transport in the intestine of WT, Tg-3A4, *Vdr*^{ΔIEpC}, and *Vdr*^{ΔIEpC}/3A4 mice. *Asbt*, *Osta*, *Ostb*, *Ibabp*, *Mrp1*, *Mrp2*, *Mrp3*, *Oatp1*, and *Oatp4* mRNAs in intestine and liver were measured by qPCR. #*P* < 0.05 compared with *Vdr*^{ΔIEpC} in same group; ##*P* < 0.01 compared with *Vdr*^{ΔIEpC} in same group.

mice might be responsible for the decreased hepatic bile acids in *Vdr*^{ΔIEpC}/3A4 mice compared with *Vdr*^{ΔIEpC} mice. There were no significant differences in expression of *Fxr* and small heterodimer partner (*Shp*) between these four groups (Fig. 6). Results of gene expression analysis thus suggested that the lower bile acid accumulation in *Vdr*^{ΔIEpC}/3A4 mice might be due to increased bile acid efflux and reduced bile acid synthesis in the liver. This change might be correlated to CYP3A4 over-metabolism of LCA and LCA detoxification in *Vdr*^{ΔIEpC}/3A4 mice.

DISCUSSION

The results of this study are summarized and the potential role of intestinal CYP3A4 in bile acid metabolism and protection against bile acid toxicity is illustrated in Fig. 7. In the intestine-specific VDR-deficient mouse, LCA-induced hepatotoxicity is more severe than in WT mice due to over-accumulation of bile acids in the liver. It was reported that reduced VDR can lead to calcium malabsorption (6), and that decreased calcium could then damage intestinal epithelia (23–25). Intestinal permeability is a key factor regulating bile acid transport and expression of target proteins (26). Deficiency of VDR in the intestine of *Vdr*^{ΔIEpC} mice leads to increased LCA toxicity in the liver after its reuptake from the intestine. Changes in intestinal structure could

increase bile acid uptake by the intestine and lead to hepatic over-accumulation of bile acids in *Vdr*^{ΔIEpC} mice as a result of LCA administration. CYP3A4 can metabolize LCA, and perhaps other bile acids, and reduce the accumulation of toxic bile acids in the liver. CYP3A4 is not significantly expressed in the livers of Tg-3A4 and *Vdr*^{ΔIEpC}/3A4 mice, and highly expressed in the intestine, in agreement with the low expression in the liver and high expression in the intestine system reported earlier for the CYP3A4-humanized mouse line (27). Therefore, any LCA metabolism by CYP3A4 is largely carried out in the intestine of *Vdr*^{ΔIEpC}/3A4 mice and not in the liver. LCA is largely excreted in the bile and feces as a sulfate conjugate (28). LCA can also be conjugated with taurine or glycine and excreted in feces or urine. Thus, LCA-induced toxicity could be decreased through increased conjugation with taurine and sulfate. It is likely that the conjugates are metabolized by bacterial bile acid hydrolase in the intestine leading to free LCA that is recirculated to the liver. However, intestinal CYP3A4 could convert LCA into hydroxylated LCA, which could further facilitate conjugation and sulfation. Oxidation of LCA by intestinal CYP3A4 could reduce circulating bile acids and alleviate LCA-induced hepatotoxicity in the *Vdr*^{ΔIEpC}/3A4 mice.

Bile and liver metabolomics revealed that taurocholic acid and TDCA, two major bile acids, were increased in the liver of *Vdr*^{ΔIEpC} mice. Urinary metabolomics demonstrated increased lithocholate-O-glucuronide, LCA acid

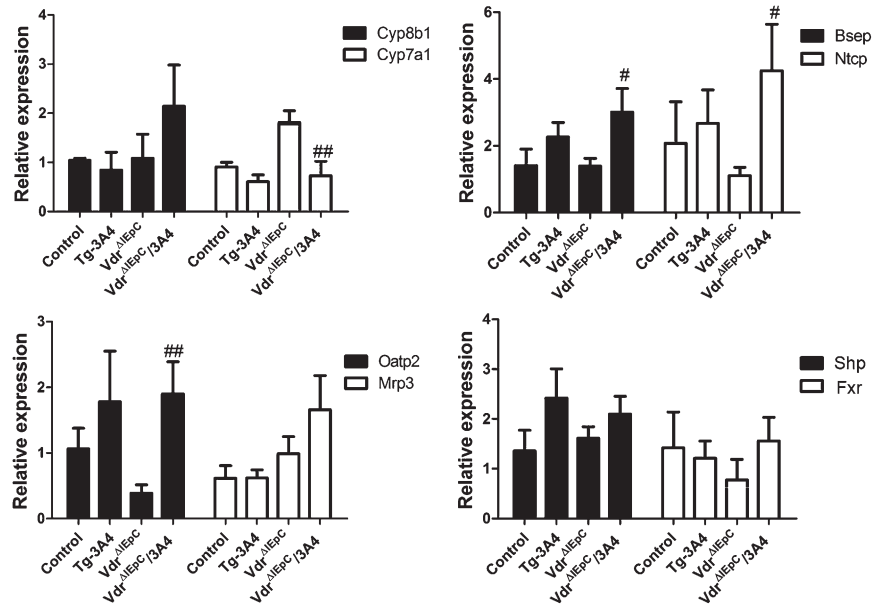


Fig. 6. Expression of mRNAs encoding enzymes responsible for bile acid synthesis and transportation in the liver of WT, Tg-3A4, *Vdr*^{ΔIEpC}, and *Vdr*^{ΔIEpC}/3A4 mice. *Cyp8b1*, *Cyp7a1*, *Bsep*, *Ntcp*, *Mrp3*, *Oatp2*, *Shp*, and *Fxr* mRNAs in liver were measured by qPCR. #*P* < 0.05 compared with *Vdr*^{ΔIEpC} in same group; ##*P* < 0.01 compared with *Vdr*^{ΔIEpC} in same group.

glycine conjugate, and hydroxylated LCA, and reduced taurine conjugates in *Vdr*^{ΔIEpC}/3A4 mice, which indicated increased metabolism and detoxification of LCA in *Vdr*^{ΔIEpC}/3A4 mice. In chronic cholestatic liver disease, hydrophobic and potentially cytotoxic bile acids accumulate in the liver (29). Thus, hepatic accumulation of taurocholic acid and TDCA and impaired metabolism of LCA in *Vdr*^{ΔIEpC} mice might contribute to the tissue degeneration in cholestatic liver disease due to the detergent effects of these bile acids.

Bile acid transport in the enterocytes basically consists of three components: 1) apical uptake of bile acids in the enterocytes largely facilitated by the uptake of conjugated bile acids in the terminal ileum via a Na⁺-dependent mechanism, such as ASBT; 2) intracellular bile acid transport in the enterocytes is mediated by cytosolic IBABP; and 3) an anion exchange mechanism for the basolateral efflux of bile acids from enterocytes, such as OSTα and OSTβ. The ileal bile acid transport system offers enormous potential as a valuable target for cholesterol/bile acid lowering

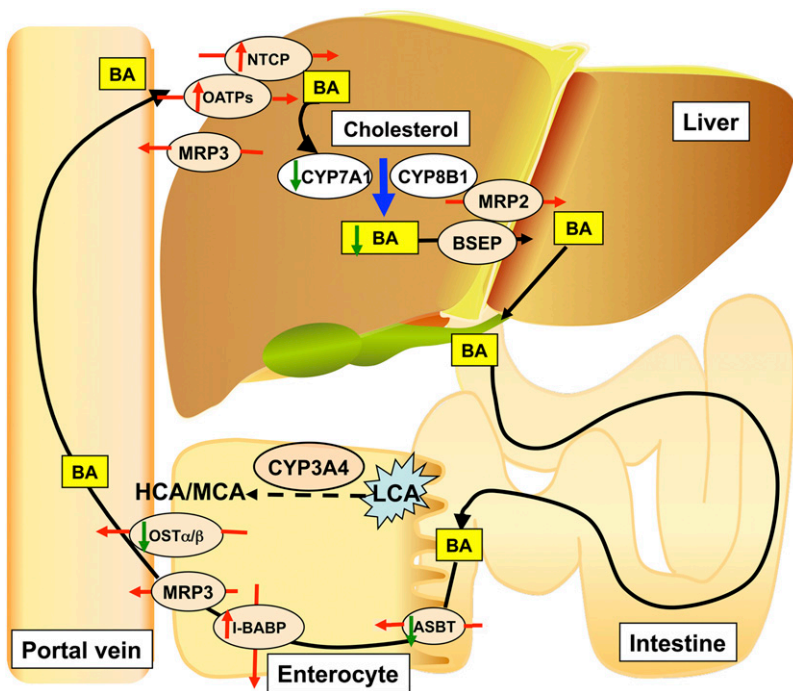



Fig. 7. Bile acid metabolic events contributing to the low accumulation of bile acids in *Vdr*^{ΔIEpC}/3A4 mice compared with *Vdr*^{ΔIEpC} mice. BA, bile acid.

therapy. Specific transporters expressed in the liver and the intestine play a critical role in driving the enterohepatic circulation of bile acids (Fig. 7). Enterohepatic circulation of bile acids is fundamentally composed of two major processes, secretion from the liver and absorption from the intestine (30). In hepatocytes, the vectorial transport of bile acids from blood to bile is carried out by NTCs and OATPs. Bile acids are then transported into the canaliculus via BSEPs and MRPs and delivered to the intestinal lumen where they are reabsorbed into enterocytes. Intestinal epithelial cells reabsorb the majority of the secreted bile acids through ASBTs and OATPs (31). Increased portal bile acid absorption as a result of elevated ASBTs in the rat in vivo by 1,25(OH)₂D₃ treatment could trigger indirect or secondary changes in hepatic transporters and enzymes due to the activation or inhibition of other nuclear receptors (32). The present results revealed decreased expression of *Oatps*, *Asbt*, and *Osta* in the intestine of *Vdr*^{ΔIEpC}/3A4 mice compared with *Vdr*^{ΔIEpC} mice. These data indicate that the absorption of bile acids in the intestine of *Vdr*^{ΔIEpC}/3A4 mice is lower than in *Vdr*^{ΔIEpC} mice. However, in the liver, there was an elevation of *Bsep* mRNA in *Vdr*^{ΔIEpC}/3A4 mice indicating increased canalicular membrane efflux, and higher expression of *Oatp2* and *Ntcp* mRNAs indicating increased hepatic bile acid uptake and efflux. Therefore, lowered hepatic bile acid accumulation in *Vdr*^{ΔIEpC}/3A4 mice might not be due to increased hepatic bile acid uptake leading to less bile acid accumulation, but due to lower enterohepatic bile acid circulation in these mice as a result of lower expression of *Oatps*, *Asbt*, and *Osta*. The mechanisms for the changes in expression of these transporters are not known and require further investigation.

In summary, the working model is that loss of intestinal VDR decreases intestinal CYP3A expression. Decreased intestinal CYP3A4 expression reduces LCA metabolism and increases the expression of intestinal transporters, which is likely not direct but due to altered bile acid metabolism and increased intestinal bile acid transport. This results in decreased bile acid loss, increased bile acid absorption into the enterohepatic circulation, and increased hepatic bile acid exposure which contributes to the increased hepatic injury. Intestine-specific VDR deficiency exacerbates LCA-induced liver cholestasis due to over-accumulation of hepatic bile acids while CYP3A4 alleviates LCA-induced hepatotoxicity through increased LCA detoxification and increased efflux of bile acids. Because intestinal VDR may contribute to the maintenance of intestinal barrier function, intestinal overexpression of CYP3A4 would be protective by detoxifying LCA and protecting intestinal barrier function. The *Vdr*^{ΔIEpC} and *Vdr*^{ΔIEpC}/3A4 mouse models could be valuable tools to investigate VDR regulation of bile acids, as well as coordination of VDR and CYP3A4 on detoxification of bile acid-induced toxicity in the gastrointestinal system. 

The authors thank Shigeaki Kato, Tokyo University, for the *Vdr*-floxed mice, and Paul A. Dawson, Wake Forest University School of Medicine, for the generous gift of the antibody to mouse ASBT.

- Haussler, M. R., C. A. Haussler, P. W. Jurutka, P. D. Thompson, J. C. Hsieh, L. S. Remus, S. H. Selznick, and G. K. Whitfield. 1997. The vitamin D hormone and its nuclear receptor: molecular actions and disease states. *J. Endocrinol.* **154**(Suppl): S57–S73.
- Bookout, A., Y. Jeong, M. Downes, R. Yu, R. M. Evans, and D. J. Mangelsdorf. 2006. Anatomical profiling of nuclear receptor expression reveals a hierarchical transcriptional network. *Cell.* **126**: 789–799.
- Li, Y. C., A. E. Pirro, M. Amling, G. Dellling, R. Baron, R. Bronson, and M. B. Demay. 1997. Targeted ablation of the vitamin D receptor: an animal model of vitamin D-dependent rickets type II with alopecia. *Proc. Natl. Acad. Sci. USA.* **94**: 9831–9835.
- Yoshizawa, T., Y. Handa, Y. Uematsu, S. Takeda, K. Sekine, Y. Yoshihara, T. Kawakami, K. Arioka, H. Sato, Y. Uchiyama, et al. 1997. Mice lacking the vitamin D receptor exhibit impaired bone formation, uterine hypoplasia and growth retardation after weaning. *Nat. Genet.* **16**: 391–396.
- Li, Y. C., J. Kong, M. Wei, Z. F. Chen, S. Q. Liu, and L. P. Cao. 2002. 1,25-Dihydroxyvitamin D(3) is a negative endocrine regulator of the renin-angiotensin system. *J. Clin. Invest.* **110**: 229–238.
- Lieben, L., R. Masuyama, S. Torreken, R. Van Looveren, J. Schrooten, P. Baatsen, M. H. Lafage-Proust, T. Dresselaers, J. Q. Feng, L. F. Bonewald, et al. 2012. Normocalcemia is maintained in mice under conditions of calcium malabsorption by vitamin D-induced inhibition of bone mineralization. *J. Clin. Invest.* **122**: 1803–1815.
- Bouillon, R., G. Carmeliet, L. Verlinden, E. van Etten, A. Verstuyf, H. F. Luderer, L. Lieben, C. Mathieu, and M. Demay. 2008. Vitamin D and human health: lessons from vitamin D receptor null mice. *Endocr. Rev.* **29**: 726–776.
- Kim, J. H., S. Yamaori, T. Tanabe, C. H. Johnson, K. W. Krausz, S. Kato, and F. J. Gonzalez. 2013. Implication of intestinal VDR deficiency in inflammatory bowel disease. *Biochim. Biophys. Acta.* **1830**: 2118–2128.
- Han, S., and J. Y. Chiang. 2009. Mechanism of vitamin D receptor inhibition of cholesterol 7α-hydroxylase gene transcription in human hepatocytes. *Drug Metab. Dispos.* **37**: 469–478.
- Han, S., T. Li, E. Ellis, S. Strom, and J. Y. Chiang. 2010. A novel bile acid-activated vitamin D receptor signaling in human hepatocytes. *Mol. Endocrinol.* **24**: 1151–1164.
- Ogura, M., S. Nishida, M. Ishizawa, K. Sakurai, M. Shimizu, S. Matsuo, S. Amano, S. Uno, and M. Makishima. 2009. Vitamin D3 modulates the expression of bile acid regulatory genes and represses inflammation in bile duct-ligated mice. *J. Pharmacol. Exp. Ther.* **328**: 564–570.
- Echchgadda, I., C. S. Song, A. K. Roy, and B. Chatterjee. 2004. Dehydroepiandrosterone sulfotransferase is a target for transcriptional induction by the vitamin D receptor. *Mol. Pharmacol.* **65**: 720–729.
- Fiorucci, S., S. Cipriani, A. Mencarelli, B. Renga, E. Distrutti, and F. Baldelli. 2010. Counter-regulatory role of bile acid activated receptors in immunity and inflammation. *Curr. Mol. Med.* **10**: 579–595.
- Hofmann, A. F. 2004. Detoxification of lithocholic acid, a toxic bile acid: relevance to drug hepatotoxicity. *Drug Metab. Rev.* **36**: 703–722.
- Makishima, M., T. T. Lu, W. Xie, G. K. Whitfield, H. Domoto, R. M. Evans, M. R. Haussler, and D. J. Mangelsdorf. 2002. Vitamin D receptor as an intestinal bile acid sensor. *Science.* **296**: 1313–1316.
- Jurutka, P. W., P. D. Thompson, G. K. Whitfield, K. R. Eichhorst, N. Hall, C. E. Dominguez, J. C. Hsieh, C. A. Haussler, and M. R. Haussler. 2005. Molecular and functional comparison of 1,25-dihydroxyvitamin D(3) and the novel vitamin D receptor ligand, lithocholic acid, in activating transcription of cytochrome P450 3A4. *J. Cell. Biochem.* **94**: 917–943.
- Johnson, C. H., A. D. Patterson, J. R. Idle, and F. J. Gonzalez. 2012. Xenobiotic metabolomics: major impact on the metabolome. *Annu. Rev. Pharmacol. Toxicol.* **52**: 37–56.
- Schulte, E. K. 1991. Standardization of biological dyes and stains: pitfalls and possibilities. *Histochemistry.* **95**: 319–328.
- Taylor, W., and M. Lesna. 1977. The hepatotoxicity of lithocholic acid in male mice. [proceedings] *Br. J. Pharmacol.* **61**: 133P–134P.
- Sonoda, J., W. Xie, J. M. Rosenfeld, J. L. Barwick, P. S. Guzelian, and R. M. Evans. 2002. Regulation of a xenobiotic sulfonation cascade by nuclear pregnane X receptor (PXR). *Proc. Natl. Acad. Sci. USA.* **99**: 13801–13806.
- Mansell, J. P., D. Shorez, D. Farrar, and M. Nowghani. 2009. Lithocholate—a promising non-calcaemic calcitriol surrogate for

- promoting human osteoblast maturation upon biomaterials. *Steroids*. **74**: 963–970.
22. Zhang, J., W. Huang, M. Qatanani, R. M. Evans, and D. D. Moore. 2004. The constitutive androstane receptor and pregnane X receptor function coordinately to prevent bile acid-induced hepatotoxicity. *J. Biol. Chem.* **279**: 49517–49522.
 23. Ballard, S. T., J. H. Hunter, and A. E. Taylor. 1995. Regulation of tight-junction permeability during nutrient absorption across the intestinal epithelium. *Annu. Rev. Nutr.* **15**: 35–55.
 24. Zhang, Y., I. L. Csanaky, L. D. Lehman-McKeeman, and C. D. Klaassen. 2011. Loss of organic anion transporting polypeptide 1a1 increases deoxycholic acid absorption in mice by increasing intestinal permeability. *Toxicol. Sci.* **124**: 251–260.
 25. Stenman, L. K., R. Holma, A. Eggert, and R. Korpela. 2013. A novel mechanism for gut barrier dysfunction by dietary fat: epithelial disruption by hydrophobic bile acids. *Am. J. Physiol. Gastrointest. Liver Physiol.* **304**: G227–G234.
 26. Soeters, P. B., M. D. Luyer, J. W. Greve, and W. A. Buurman. 2007. The significance of bowel permeability. *Curr. Opin. Clin. Nutr. Metab. Care.* **10**: 632–638.
 27. Yu, A. M., K. Fukamachi, K. W. Krausz, C. Cheung, and F. J. Gonzalez. 2005. Potential role for human cytochrome P450 3A4 in estradiol homeostasis. *Endocrinology*. **146**: 2911–2919.
 28. Palmer, R. H., and Z. Ruban. 1966. Production of bile duct hyperplasia and gallstones by lithocholic acid. *J. Clin. Invest.* **45**: 1255–1267.
 29. Fischer, S., U. Beuers, U. Spengler, F. M. Zwiebel, and H. G. Koebe. 1996. Hepatic levels of bile acids in end-stage chronic cholestatic liver disease. *Clin. Chim. Acta.* **251**: 173–186.
 30. McCarthy, T. C., X. Li, and C. J. Sinal. 2005. Vitamin D receptor-dependent regulation of colon multidrug resistance-associated protein 3 gene expression by bile acids. *J. Biol. Chem.* **280**: 23232–23242.
 31. Alrefai, W. A., and R. K. Gill. 2007. Bile acid transporters: structure, function, regulation and pathophysiological implications. *Pharm. Res.* **24**: 1803–1823.
 32. Maeng, H. J., M. R. Durk, E. C. Chow, R. Ghoneim, and K. S. Pang. 2011. 1 α ,25-dihydroxyvitamin D₃ on intestinal transporter function: studies with the rat everted intestinal sac. *Biopharm. Drug Dispos.* **32**: 112–125.